pss

+++rapid
research
letters+++

www.pss-rapid.com

Comparing the weak and strong gate-coupling regimes for nanotube and graphene transistors

I. Heller, S. Chatoor, J. Männik, M. A. G. Zevenbergen, C. Dekker, and S. G. Lemay*

Kavli Institute of Nanoscience, Delft University of Technology, Lorentzweg 1, 2628 CJ Delft, The Netherlands

* Corresponding author: e-mail s.g.lemay@tudelft.nl

We present an experimental and theoretical comparison of the weak and strong gate-coupling regimes that arise for carbon nanotube (CNT) and graphene field-effect transistors (FETs) in back-gated and liquid-gated configuration, respectively. We find that whereas the back-gate efficiency is suppressed for a liquid-gated CNT FET, the back gate is still effective in case of a liquid-gated graphene FET. We calculate the gate-induced Fermi-level shifts and induced charge densities. In both strong and weak coupling regimes, nonlinearities occur in the gate dependence of these parameters, which can significantly influence the electronic transport.

1 Introduction Carbon nanotubes (CNTs) and graphene are highly interesting materials for application in field-effect transistors (FETs), both for circuitry and as sensor elements in gas or liquid [1–4]. A range of source, drain, and gate electrode configurations have been demonstrated in which the coupling of the channel to the gate varies from weak, such as in a classic back-gated layout [5, 6] (Fig. 1a), to strong such as in an electrolyte-gated layout [7–9] (Fig. 1b). Here we experimentally study the regimes of strong and weak gate coupling for CNT and graphene FETs. In addition, we calculate the gate-induced changes in Fermi level and charge density and show that nonlinear behavior occurs depending on the gate geometry.

2 Liquid gating versus back gating We fabricated CNT and graphene FETs on oxidized silicon wafers as sketched in Fig. 1a and b. The fabrication process was described previously [10–12]. Figure 1c and d show typical ambipolar source–drain current (I_{sd}) as a function of both back-gate potential (V_{bg}, red) and liquid-gate potential (V_{lg}, black) measured for the same CNT (Fig. 1c) and graphene FET (Fig. 1d). The large difference in voltage range between the liquid-gated and the back-gated configuration strikingly illustrates the difference in gating efficiency, as reported previously [7–9]. The difference in

gate-coupling strength can be estimated by comparing the voltage axis scaling when changing from a back-gated to a liquid-gated layout. By this criterion, the CNT and graphene devices of Fig. 1 are, respectively, 13 and 180 times more weakly coupled to the back gate than to the liquid gate.

To further evaluate the gate coupling strength, we use the simple equivalent circuit depicted in the inset of Fig. 1d [7, 8, 13]. Here, the total capacitance to the gate is represented by the geometrical capacitance (C_G) in series with the quantum capacitance (C_Q). The applied gate potential V_g drops over these two capacitances as $V_g = V_{es} + V_{ch}$, with V_{es} the electrostatic potential drop and V_{ch} the chemical potential drop. We estimate the gate coupling $\alpha = \Delta V_{ch}/\Delta V_g$ using rough estimates for C_Q and C_G (although we use constant values here, C_Q and C_{lg} are in fact gate dependent, as discussed further below). We take $C_{bg,NT} = 0.04$ fF/µm, $C_{Q,NT} = 0.4$ fF/µm, and $C_{lg,NT} = 6$ fF/µm for back-gate, quantum, and liquid-gate capacitances for a CNT, and $C_{bg,gr} = 0.1$ fF/µm², $C_{Q,gr} = 12$ fF/µm², and $C_{lg,gr} = 700$ fF/µm², for back-gate, quantum and liquid-gate capacitances for graphene (see Supporting Information, online at www.pss-rapid.com). Using these estimates, we see that α is about 0.1 and 0.008 for the weakly-coupled back gate for CNTs and graphene,
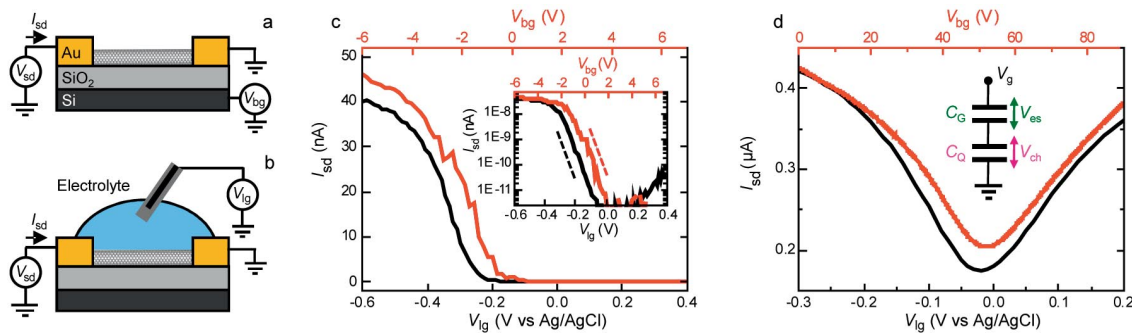
Figure 1 (online colour at: www.pss-rapid.com) Back gating versus liquid gating. (a, b) Device schematics for a back-gated FET and a liquid-gated FET, respectively. (c) $I_{sd}(V_{lg})$ (solid black line) and $I_{sd}(V_{bg})$ (solid red line) measured on the same CNT FET in liquid-gated and back-gated configurations, respectively. The inset shows the same data on a logarithmic scale, where slopes of 60 mV/decade (black dashed line) and 0.8 V/decade (red dashed line) have been indicated. (d) $I_{sd}(V_{lg})$ (solid black line) and $I_{sd}(V_{bg})$ (solid red line) measured as in (c) for a single layer graphene FET. The inset shows the circuit diagram of the gate capacitance. The applied source−drain potential V_{sd} in (c) and (d) is 10 mV and 1 mV, respectively.

respectively, while it is 0.94 and 0.98 when the same devices are gated using a liquid gate. The ratio of α in back-gated over liquid-gated configuration is thus estimated as 10 and 120 for CNTs and graphene, respectively, in good agreement with the experimentally obtained ratios from Fig. 1. A coupling near unity, indicating a nearly ideally strong gate coupling, is indeed experimentally confirmed by the sub-threshold slope close to the maximum value of 60 mV/decade for the liquid-gated CNT device of Fig. 1c (see dashed lines in inset) [8, 10].

A more direct comparison of back-gate and liquid-gate efficiency can be made when both gate types are employed simultaneously, as schematically depicted in Fig. 2a. Figure 2b shows $I_{sd}(V_{lg}, V_{bg})$ for a bilayer graphene device measured as function of both V_{lg} and V_{bg}. From the slope of the dashed white line (which tracks the minimum of conductance), we find that the ratio of the gate efficiencies is 154 ± 5, in good agreement with our estimate of 180 obtained when liquid gate and back gate were applied separately.

The situation is different for a CNT FET. Whereas the back gate still functions well when a liquid gate is applied on top of a graphene sheet (cf. Fig. 2b), the back-gate efficiency is largely suppressed in the case of a liquid-gated CNT FET. This can be attributed to the presence of the electrolyte in proximity to the CNT, which intercepts electric field lines that would otherwise pass from the back gate to the CNT. The suppression of back-gate efficiency by the liquid gate can be exploited in a more complex device layout to separately control the doping level along different sections of one CNT, as we demonstrated previously [12]. Figure 2c depicts such a CNT FET for which the central section is in direct contact with the electrolyte, but the contact regions are separated from the electrolyte by a layer of PMMA. Figure 2e shows $I_{sd}(V_{lg}, V_{bg})$ measured for such a partially liquid-gated CNT FET. Whereas the back-gate efficiency along the liquid-gated section of the CNT is negligible, the back gate significantly affects the doping level of the PMMA-covered sections. This can be observed for large positive V_{bg} in Fig. 2e, where conduction through

the PMMA-covered sections becomes pinched off. As illustrated by the energy diagram in Fig. 2d, both entirely p-doped (ppp) and pnp configurations can thus be obtained. From the slope of the white dashed line (which approximately tracks the center of the band gap), we estimate that the ratio of liquid-gate to back-gate coupling here is ~500. This large difference in gate coupling, which corresponds to a decreased back-gate efficiency for a liquid-gated CNT FET, is indeed significantly larger than the factor of 13 difference found previously in Fig. 1c.

3 Effect of gate-coupling strength on transport The previous discussion illustrated the gating in different gate-coupling regimes. We now theoretically consider the implications of the gate efficiency for transport properties. The strength of the gate coupling determines the induced Fermi-level shifts, which in turn determines the number of charge carriers N_C present in the channel [13]. Because
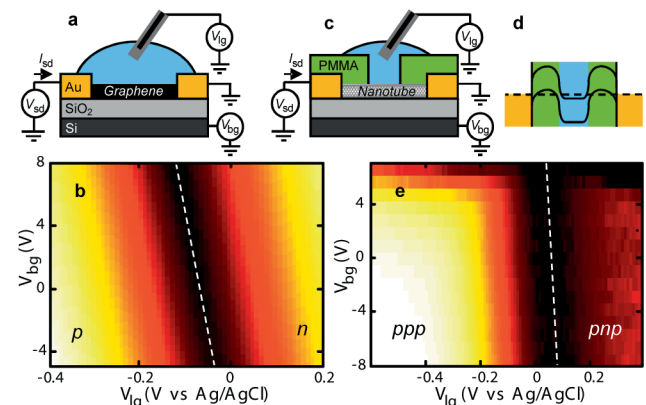

Figure 2 (online colour at: www.pss-rapid.com) Combined liquid and back gating. (a) Device schematic for the bilayer graphene device measured in (b). (b) I_{sd} measured as a function of applied V_{lg} and V_{bg}. The color scale is linear. (c) Device schematic of the nanotube device measured in (e). (d) Band diagram of a possible pnp-gated situation. (e) I_{sd} measured as function of applied V_{lg} and V_{bg}. The color scale is logarithmic.

CNTs and graphene have non-constant densities of states $\rho(E)$, both $E_F(V_g)$ and $N_C(V_g)$ can be nonlinear functions of V_g. In Fig. 3 we calculated $\Delta E_F(V_g)$ and $\Delta N_C(V_g)$ for a liquid-gated layout, a back-gated layout, and the intermediate regime of a top-gated layout, to show that the respective V_g dependencies of these transport parameters behave qualitatively different in weak and strongly coupled gate regimes. The calculations use $\Delta E_F(V_{lg})/e = V_{lg}C_G/(C_Q(E_F) + C_G)$. $C_Q(E_F)$ depends on the density of states at the Fermi-level according to $C_Q(E_F) = e^2 \Delta N_C/\Delta E_F$, with $N_C(E_F) = \int f(E - E_F) \rho(E) \, dE$, and $f(E)$ the Fermi–Dirac distribution. The electrostatic capacitance in liquid-gated layout, C_{dl}, also slightly varies with applied V_{lg}, which we ignore here for simplicity. Figure 3 shows numerical solutions to the equations described above. For graphene (blue lines) we used $\rho(E) = 2|E|/\hbar^2 v_F^2 \pi$, and for CNTs (red lines) we have adopted procedures of Ref. [14] to calculate $\rho(E)$ for a 2 nm diameter semiconducting CNT.

In the strongly coupled regime, $C_{dl} \gg C_Q$, and C_Q dominates the total gate capacitance (and since $C_Q \approx 0$ within the band gap of a CNT, this situation easily arises). As a result, $\Delta E_F \propto V_{lg}$, as illustrated by the quite linear $\Delta E_F(V_{lg})$ curve close to the ideal limit $\Delta E_F = V_{lg}$ (black dashed line). At higher V_{lg} however, the ratio of C_Q/C_{dl} increases (cf. Fig. 3d), leading to an increased departure from ideal gate coupling and a slightly sub-linear $\Delta E_F(V_{lg})$. $\Delta N_C(V_{lg})$ (Fig. 3g) reveals a much stronger nonlinear behavior (roughly parabolic for graphene). The opposite behavior is observed in the weakly coupled regime (cf. Fig. 3c, f, i). Since the gate capacitance here is dominated by the constant C_{bg}, ΔN_C now increases linearly with V_{bg}. ΔE_F on the other hand varies roughly as $V_{lg}^{1/2}$, as opposed to linearly in the strongly coupled regime. Finally, Fig. 3b, e, h show ΔE_F, C_Q/C_{tg} and ΔN_C for a solid-state top gate that

is separated from the graphene sheet by a 5 nm SiO$_2$ layer. In this intermediate regime, C_Q/C_{tg} varies roughly between 1 and 10, causing nonlinear behavior in both E_F and N_C.

The abovementioned dependencies of E_F and N_C on V_g reveal qualitatively different behavior in the different gate-coupling regimes. Strong nonlinearities are observed in gate-voltage ranges that are commonly accessed experimentally. These parameters are often crucial when interpreting transport data in terms of device mobility, doping level, and noise properties. Additionally, the observed nonlinearities can play a role in nonlinear transport behavior at high V_g, for which mechanisms based on scattering or contact effects have been proposed previously [15–17].

4 Conclusion We have studied the differences in gate coupling for CNT and graphene FETs with various device layouts and their implications for transport. For a liquid-gated graphene FET, the back gate remains effective, whereas a liquid gate surrounding a CNT severely decreases the back-gate efficiency. This implies that charges in the oxide will have a larger impact on a graphene sheet covered by liquid than on a CNT. We demonstrated experimentally that the back gate can be used to shift the liquid-gate potential at which the Dirac point occurs for a graphene sheet or to independently modulate the conductance of different sections of a partially liquid-gated FET. Depending on the gate coupling strength, transport parameters such as the charge carrier density and the position of the Fermi level can exhibit strongly nonlinear dependence on applied gate potential. For strong coupling, E_F varies linearly with V_g, whereas N_C varies linearly with V_{lg} for weak coupling. In all other situations nonlinearities occur.

Figure 3 (online colour at: www.pss-rapid.com) Calculated effect of gate-coupling strength on transport for CNTs (red) and graphene (blue). E_F, C_Q/C_{tg} and N_C calculated as function of V_g for: (a, d, g) a liquid gate using $\varepsilon = 80$ and $d = 1$ nm; (b, e, h) a top gate using $\varepsilon = 4$ and $d = 5$ nm; (c, f, i) a back gate using $\varepsilon = 4$ and $d = 300$ nm, respectively.

References

[1] D. R. Kauffman and A. Star, Angew. Chem. Int. Ed. **47**, 6550 (2008).
[2] D. R. Kauffman and A. Star, Chem. Soc. Rev. **37**, 1197 (2008).
[3] F. Schedin et al., Nature Mater. **6**, 652 (2007).
[4] P. K. Ang et al., J. Am. Chem. Soc. **130**, 14392 (2008).
[5] S. J. Tans et al., Nature **393**, 49 (1998).
[6] K. S. Novoselov et al., Science **306**, 666 (2004).
[7] M. Krüger et al., Appl. Phys. Lett. **79**, 1291 (2001).
[8] S. Rosenblatt et al., Nano Lett. **2**, 869 (2002).
[9] A. Das et al., Nature Nanotechnol. **3**, 210 (2008).
[10] J. Männik et al., Nano Lett. **8**, 685 (2008).
[11] I. Heller et al., Nano Lett. **8**, 591 (2008).
[12] I. Heller et al., Nano Lett. **9**, 377 (2009).
[13] I. Heller et al., J. Am. Chem. Soc. **128**, 7353 (2006).
[14] J. W. Mintmire and C. T. White, Phys. Rev. Lett. **81**, 2506 (1998).
[15] B. Huard et al., Phys. Rev. B **78**, 121402 (2008).
[16] E. H. Hwang et al., Phys. Rev. Lett. **98**, 186806 (2007).
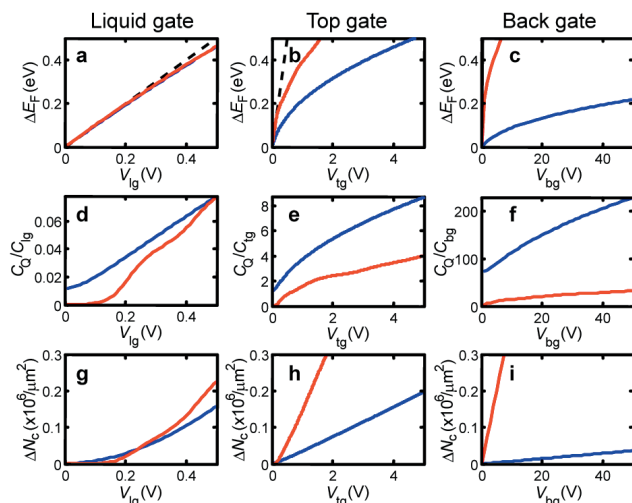[17] F. Chen, J. Xia, and N. Tao, Nano Lett. **9**, 1621 (2009).